DIFFRACTION BY BUILDING CORNERS AT 28 GHz: MEASUREMENTS AND MODELING

by

Peter A. Tenerelli

Thesis submitted to the Faculty of the
Virginia Polytechnic Institute and State University
in partial fulfillment of the requirements for the degree of

MASTER OF SCIENCE
in
Electrical Engineering

APPROVED:

_____
Dr. Charles Bostian, Chair

_____ _____
Dr. Ira Jacobs Dr. Warren Stutzman

June 3, 1998
Blacksburg, Virginia

Key words: diffraction, propagation, LMDS, 28 GHz, measurements

DIFFRACTION BY BUILDING CORNERS AT 28 GHz: MEASUREMENTS AND MODELING

Peter A. Tenerelli

(ABSTRACT)

This thesis presents the results of a 28 GHz continuous-wave (CW) diffraction measurement campaign in the Washington, DC area. It describes the measurement approach including information on equipment and testing methods. Also described are the various parameters that affected the diffraction loss. Observed diffraction losses showed little dependence on polarization and building material. For diffraction angles greater than 5°, a simple linear equation was fit to the data and accurately describes the diffraction loss. A logarithmic equation describes the dependence at smaller angles. The model developed shows very good agreement with theory and other measurements.

Also included are an overview of the fixed wireless industry, a discussion of system design issues, and a review of the historical and mathematical development of diffraction theory.

Acknowledgments

I would like to express my sincere thanks to my academic advisor, Dr. Charles Bostian. His guidance, patience and expertise has made my graduate experience meaningful and fulfilling. My relationship with committee members Drs. Ira Jacobs and Warren Stutzman began in the classroom and evolved into discussions about navigating diffraction theory, my experiment design, and finally detailed suggestions for clarifying and improving the final thesis. I express my thanks to them for their important contributions to my graduate program.

I would like to thank my employer, LCC International, Inc., and especially my boss, Guy Jouannelle who have provided me with the flexibility and tools to allow me to be successful in my graduate program.

I am grateful for the constant support, encouragement, and critique from my wife Candice. Her presence made the uphill portions of my academic journey seem much less daunting.

These acknowledgments would be incomplete without thanks to those who made long term commitments to my success and set me on the right course for perseverance and success. I give my thanks to my parents for teaching me the value of education, the difference between right and wrong and value of one's character. I also wish to thank my first and long time boss, Dr. Elliot Rosen, for teaching me the tools of patience and curiosity that motivated and sustained me in my graduate school experience.

TABLE OF CONTENTS

LIST OF FIGURES

1. Introduction

1.1. Content and Organization of Thesis

This thesis describes the bending of radio waves around objects or “diffraction”. Specifically, it addresses diffraction around building corners at 28 GHz. The theory behind this phenomenon is presented along with results from a recent measurement campaign. Chapter 1 discusses telecommunications market conditions and the “fixed wireless” industry. Also covered are system design issues. Chapter 2 introduces diffraction theory beginning with a historical perspective followed by the mathematical formulation of diffraction losses. Chapter 3 describes the diffraction measurement campaign including measurement goals and experiment design. Chapter 4 presents, discusses, and interprets the measurement results and develops a mathematical model that characterizes the measured diffraction losses. Chapter 5 summarizes the findings and concludes the thesis.

A few comments regarding terminology are appropriate at this point. This thesis is concerned with the additional loss that an obstructing building corner introduces into a radio link. By "additional loss" we mean loss in excess of free-space spreading loss. Following common usage in the communications industry, we have termed this additional loss "diffraction loss." A better term would be "excess path loss”, since "diffraction loss" means something different to electromagnetic theorists; see Section 4.2.4 for a discussion of the difference. "Excess path loss" is rarely used in the literature, and we employ the term here only when necessary to distinguish explicitly between "excess path loss" and the "diffraction loss" of electromagnetic theory.

1.2. Contributions

This thesis makes the following contributions:

- Measurement of diffraction losses at 28 GHz for various 90° building corners and building materials. Consistent measurement results are used to validate mathematical models.
- Development of a simplified mathematical model that characterizes the diffraction measurement results. Good agreement with theory is shown.
- Comparison of measurement results to theory and to measurements made by other researchers.

The next sub-sections discuss the fixed wireless industry and system design issues.

1.3. Fixed Wireless Industry

1.3.1. Market Conditions

In recent years, the telecommunications industry has become increasingly competitive because of several legal, political, and social factors. In particular, many communications ministries worldwide have introduced competition into a marketplace that was once monopolistic. In many countries, mobile communications service was the first telecommunications industry to be opened to competition. More recently, governments are allowing competition in telephone and data services that directly serve homes and businesses. This market segment is known as the "local loop" while the generic name for the non-mobile radio segment is "fixed wireless". Due to the high cost of building a wireline based local loop infrastructure, many companies desire to offer "wireless local loop" (WLL) service. In a WLL system, businesses and homes are connected to this new network by radio links rather than wires, cables, or fibers. In

response to this desire, there have been many radio spectrum (re) allocations throughout the world.

1.3.2.Spectrum Allocations

In order to provide enough bandwidth for high data rate communications services, there has been a (re) allocation of spectrum worldwide for frequencies with wavelengths near one centimeter. Depending on the geographic location in the world, the spectrum allocated to such services typically is in the range between 10 GHz and 40 GHz. This thesis focuses on diffraction at 28 GHz. In the United States, the 28/31 GHz and 24 GHz bands have been allocated to "multipoint distribution service" (MDS). At the 24.5 GHz band, approximately 1 GHz of spectrum is licensed to the Teligent Corp. of Alexandria, VA. They hold these licenses in 74 cities throughout the United States. In the 28 and 31 GHz bands, the Federal Communications Commission (FCC) recently auctioned licenses in February 1998. For details, see Table 1. The services at 24 and 28/31 GHz are often referred to as "Local Multipoint Distribution Service" (LMDS). Note that unlike other radio service licenses, the LMDS operator is not restricted to offering a certain type of service to the customer (i.e. voice, data, or video). Although LMDS' frequency band is much higher than that of traditional mobile radio systems, the radio network architectures are similar.

Table 1 LMDS Band Plan

Frequency (GHz)	Licensee	Remarks
27.50 – 28.35	A Band	Primary Service
29.10 – 29.25	A Band	Shared with Mobile Satellite Services (MSS)
31.075 – 31.225	A Band	Primary Service
31.000 – 31.075	B Band	Co-primary with incumbent point-to-point licensees
31.225 – 31.300	B Band	Co-primary with incumbent point-to-point licensees

1.4. System Design Issues

This section reviews LMDS system design issues including network architecture, propagation limitations in an LMDS system, and the importance of characterizing diffraction.

1.4.1.Network Architecture

The layout of an LMDS system is similar to cellular radio systems. LMDS will employ multiple base stations to provide service to a given geographic area and frequency reuse will play an important role in maximizing system capacity. The size of the "cell" or base station coverage area will be much smaller than in cellular, with a maximum radius of approximately four kilometers. LMDS systems will use fixed position antennas, mostly rooftop mounted, at both the customer location and the base station or "hub". The customer antenna will be a compact, highly directional antenna while the base station antennas will be either omnidirectional or sectored.

1.4.2.Limitations

Although there are many similarities to cellular radio, several relevant factors are different in an LMDS system design and implementation. There are significant limitations to consider when using the upper microwave frequency bands. These will be discussed later in this section. Probably the greatest attraction to the LMDS licenses is the sheer amount of radio spectrum being licensed to one operator. The winner of the "A" band license in each Basic Trading Area (BTA) will have the right to use over 1000 MHz of spectrum! As companies put together business plans to make a case for LMDS, the immense capacity and number of possible uses of all that spectrum is the main pro.

At the same time, there are major propagation problems to overcome. Since losses (attenuation) due to propagation through buildings and other obstacles is prohibitively large, LMDS is generally expected to be a line of sight (LOS) microwave radio system. That means that there are no obstructions between the transmit and receive antennas. This constraint poses a serious engineering challenge to the system designer with regard to the placement and relative position of the antennas. To compound the problem, there is a very high attenuation due to propagation through precipitation at this frequency band. This translates to smaller radio coverage areas, more radio distribution hubs, and therefore higher infrastructure costs. It is the responsibility of the system designer to understand and mitigate the effects of these impediments.

1.4.3.Importance of Characterizing Diffraction

In the previous section, we have identified several challenges to the LMDS system designer:

a) High attenuation when propagating through obstacles
b) High attenuation when propagating through precipitation

There is nothing that the system designer can do about the second factor except to keep the path lengths short -- this restriction is based on the irrefutable laws of physics. Examining the first factor, it is clear that one cannot move buildings in the interest of improved radio service. But one can investigate what happens to a radio signal when it bends around the corner of buildings. We would like to characterize mathematically this radio propagation phenomena known as diffraction.

The LMDS system operator knows that providing LOS coverage to all areas near all hubs is not practical. At the same time, the operating company will want to make the LMDS system cost effective, serving as many customers as possible and thereby maximizing revenues. In order to meet this objective, the questions that need to be answered are the

following: Exactly which customers *can* be served without a line of sight between the hub and customer antenna? How can this be predicted rather than relying on field measurements at each customer site? There are two main propagation mechanisms that can provide service to non-LOS areas. They are diffraction and reflection.

While characterizing reflections from buildings and other objects is a useful means for predicting received radio signals at a given point, it appears that the diffraction mechanism may provide a more reliable means (less attenuation) of transporting the radio signal than reflections. This is especially true when the radio wave has to "bend" only slightly (the diffraction angle is small) to reach the receive antenna. A series of measurements at 28 GHz in [Sei95] found that in the non-LOS case, most of the strongest signals were received when the receive antenna was pointed in the direction of the transmitter. This implies that the diffraction mechanism is the primary means of transporting the best signal to the receive antenna. This thesis will focus on diffraction and not discuss reflections.

An accurate characterization of the diffraction propagation mechanism can be used in an automated radio network planning tool. This tool would utilize a terrain database and a three-dimensional building database at the core of its calculations. In the absence of such a tool, the diffraction calculation can be used to determine the feasibility of potential customer antenna locations that have near-LOS paths with a single obstacle on the path. With the ability to predict the effects of diffraction, the radio system operator can rapidly predict the feasibility of non-LOS paths and provide service to these customers without costly field measurements.

The next chapter reviews diffraction history and introduces the mathematical foundation for diffraction theory.

2. Review of Diffraction History and Theory

This chapter reviews the historical and theoretical aspects of diffraction. It discusses scientific theories starting with early notions of optics up to the Geometrical Theory of Diffraction (GTD) and its enhancements.

Visible light was the subject of early scientific studies in electromagnetics. Light was studied as early as the third century BC when there were two distinct hypotheses. The first was proposed by the Pythagoreans and held by Euclid among others. Their hypothesis assumed that light was a fluid that emanated from the eye and traveled along rectilinear paths toward objects. The Atomists held the other hypothesis that stated there was an emission of a *simulacra* or image from the object to the eye. [Cro94]

It is the Italian Jesuit Francesco Maria Grimaldi who is credited as the first observer to document the diffraction phenomenon. In [Gri65], he stated that "[t]he light propagates or scatters not only directly, by refraction and reflection, but also in a fourth way, by diffraction." Grimaldi demonstrated the phenomenon by conducting two experiments. The first involved allowing light to pass through a small aperture with the direct paths blocked by an opaque body. He noticed that light still bypassed the opaque body and appeared just outside the rectilinear path area. The second experiment, he found that a cone of light passed through two very small apertures produced a spot of light larger than predicted by the principles of rectilinear light or geometrical optics (GO).

Although Grimaldi identified diffraction, he was unable to formulate a theoretical explanation. It is interesting to note that Grimaldi was opposed to the corpuscular theory of light where it is thought of as a swarm of particles. He believed that light was a fluid, which was contrary to the beliefs of subsequent scientists including Newton. His experiments were published posthumously in 1665 in the book, *De Lumine* where he named the phenomenon based on the Latin verb *diffringere* meaning "to break in different directions." [Cro90]

In the late seventeenth century, Christian Huygens [Huy90] and Isaac Newton [New04] began their work on light theory. Newton was a staunch supporter of the corpuscular theory of light. This theory could explain the geometrical optics phenomena such as rectilinear propagation, reflection and refraction. However, this corpuscular theory was unable to explain the diffraction and interference phenomena. [Cro94] Newton did quote Grimaldi's work in his book *Optiks* [New04], but due to his strong feelings for the corpuscular theory, he essentially ignored Grimaldi's findings. In fact, Newton even gave a new name to diffraction: *inflexion*, from the Latin, *inflecto*, meaning to bend. Thus, the term "diffraction" disappeared from use during the time of Newton and did not reappear until around 1815 when Augustin J. Fresnel re-introduced it. [Cro94]

In 1690, Huygens [Huy90] made a major contribution to understanding diffraction. His elementary-wave principle stated that a new or secondary wavefront was the envelope of elementary waves emanating from the primary wavefront. Although he could not explain diffraction or how the elementary waves added up, he was able to provide this qualitative assessment. It was 150 years later that Sir George Stokes [Sto49] noted that no backward direction wave (CC) was created from the primary wave (AA). See Figure 1. This led to the familiar cardiod representation of the secondary wave. [Cro94] After the period of Huygens and Newton, one hundred years would pass before more substantial progress was made in the explanation of diffraction. [Cro94]

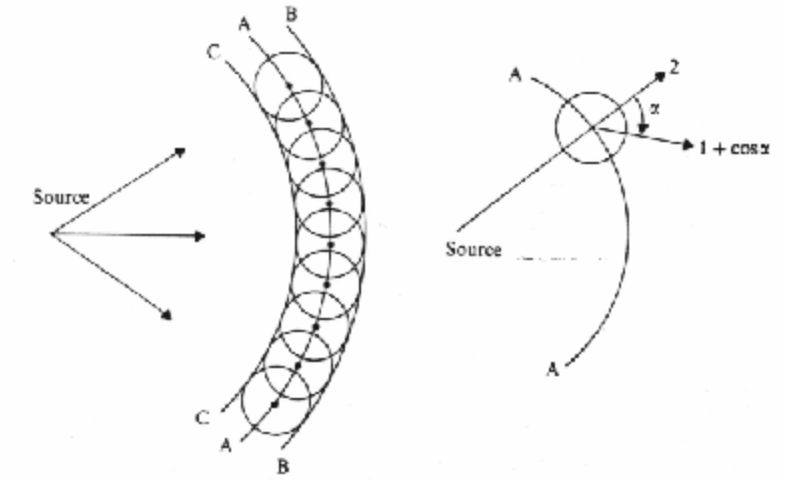

Figure 1 Huygens elementary-wave principle, taken from [Gri87]

In 1802, Thomas Young [You01] made a fundamental step in the interpretation of diffraction. He described light in the ondulatory framework where light is thought of as a wavelike perturbation propagating in a medium. He stated that diffraction is the result of the interference of two waves. The first one exists only in the lit region and follows free space propagation laws, while the second, the diffracted wave, originates at the illuminated geometrical discontinuity. Young assumed that the first wave was discontinuous at the boundary of the geometrical shadow and that the diffracted wave was continuous everywhere. Although his works were fundamental to the theory of diffraction, his contemporaries were “astonished” and clearly not ready for such “bold speculations” [Hel73] made by Young. The perceived credibility of his ideas was also hindered by the fact that they were expressed qualitatively. [Cro94].

A.J. Fresnel made important contributions to the wave theory of light in 1815 [Fre66] when he combined Huygens principle with interference. He suggested that the phase of the elementary wave be taken into account when calculating the secondary wavefront. This effectively changed the principle of elementary waves and became known as the Huygens-Fresnel principle. [Cro94]

This section will provide a mathematical explanation of the Huygens-Fresnel principle including the contribution of Stokes. [Gri87] Refer to Figure 2. In order for no backward wave CC to be created, the secondary wavelets cannot have uniform amplitude in all directions. If α is the angle of interest, then the relative amplitude is proportional to (1 + cos α). To examine the contribution of a wavelet Y at some distant point W, refer to Figure 2, part a.

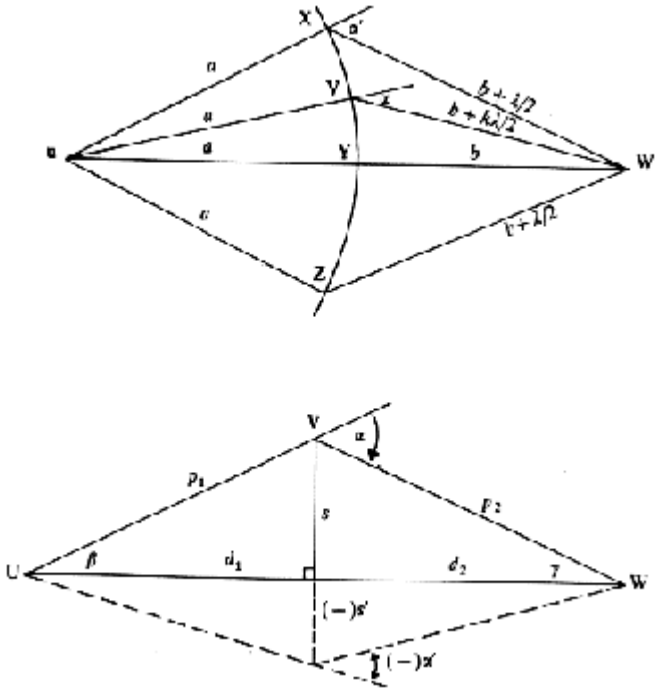

Figure 2 Geometry of Huygens-Fresnel principle. Taken from [Gri87].

Y will contribute an amplitude at W that is proportional to 1 + cos 0° = 2 (phase reference 0°). Wavelet V's amplitude is proportional to (1 + cos α) < 2 with a phase lag of kπ radians where 0<k<1. Wavelet X's amplitude is proportional to 1 + cos α' with a phase lag of π radians. This process is repeated over the entire wave front.

Assuming $s << d_1, d_2$ and $s >> \lambda$, (see Figure 2, part b) the difference between the direct and diffracted paths, the "excess path length", is

$$\Delta = \frac{s^2}{2}\frac{d_1 + d_2}{d_1 d_2} \qquad \textbf{(1)}$$

and the phase difference is

$$\phi = \frac{2\pi}{\lambda}\Delta = \frac{\pi}{2}\frac{2(d_1 + d_2)s^2}{\lambda d_1 d_2} = \frac{\pi}{2}\upsilon^2 \quad \textbf{(2)}$$

where ν is an auxiliary parameter used to normalize the calculations.

Under the same assumptions,

$$\alpha = \beta + \gamma = \frac{s}{d_1} + \frac{s}{d_2} \quad \textbf{(3)}$$

or

$$s = \alpha\frac{d_1 d_2}{d_1 + d_2} \quad \textbf{(4)}$$

where α, β, and γ are angles shown in Figure 2, part b and noting that tan x ≈ x.

Combining equations, we arrive at the expression

$$\upsilon = s\sqrt{\frac{2(d_1 + d_2)}{d_1 d_2 \lambda}} = \alpha\sqrt{\frac{2d_1 d_2}{(d_1 + d_2)\lambda}} \quad \textbf{(5)}$$

and the amplitude and phase of the wave are given in terms of ν. [Gri87]

The auxiliary parameter is often used in modeling the diffracting object as an infinitely thin "knife edge" and the loss is calculated by solving the "Fresnel integral", F(ν):

$$F(\upsilon) = \frac{(1+j)}{2}\int_{\upsilon}^{\infty} e^{((-j\pi t^2)/2)}dt \quad \textbf{(6)}$$

which is often evaluated using tables, graphs, or numerical solutions. [Rap96].

More than a half century passed before Kirchhoff devised his scalar theory of diffraction [Kir82] that confirmed Fresnel's diffraction theory. His formulation is based on a scalar wave from a point source impinging on an opaque screen with an aperture. The layout of his experiment is shown in Figure 3. The expression for u(P), the total field at point P is given by

$$\mathbf{u(P)} = \frac{1}{4\pi} \int_{A+B+C} \left[u \frac{\partial}{\partial x}\left(\frac{e^{-jks}}{s}\right) - \frac{e^{-jks}}{s}\frac{\partial u}{\partial n} \right] dS \qquad \mathbf{(7)}$$

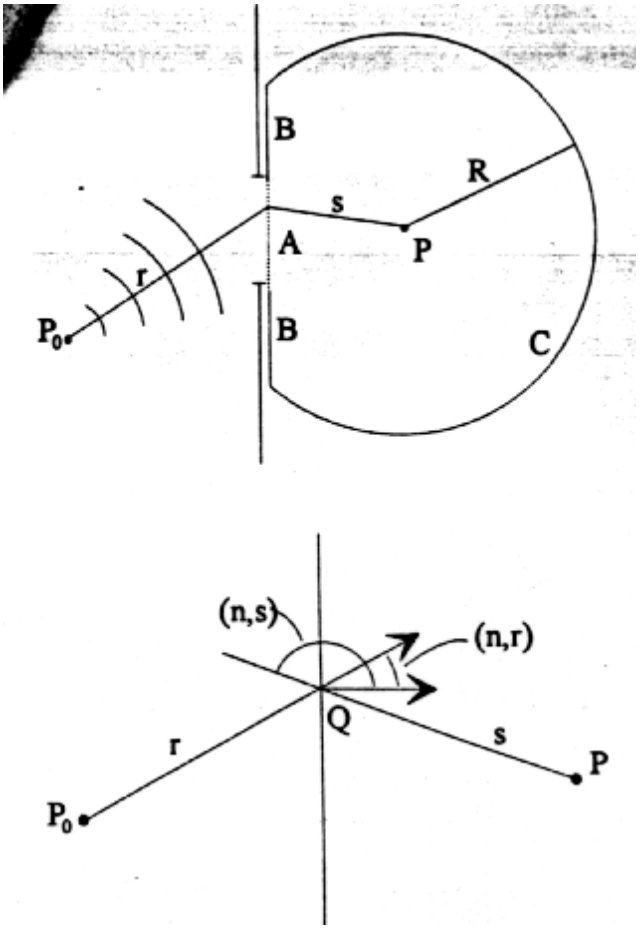

Figure 3 Geometry of Kirchhoff's diffraction at an aperture in an opaque screen, of a monochromatic wave originated by a point source at position Po. Taken from [Cro94]

This approach is used to find the field behind the screen. The inherent assumption is that the field over the aperture is not perturbed. This, incidentally, is the basic idea behind the aperture antenna technique. [Cro94]

In 1896, Sommerfeld [Som96] developed a rigorous solution for diffraction by a perfectly conducting half plane. He showed that the wave in the shadow region is a cylindrical wave that originates at the edge of the half plane. In the lit region, Sommerfeld showed that the wave could be expressed as the summation of a cylindrical wave and the incident plane wave. It was later found that the Kirchhoff diffraction theory could be expressed as two parts: the incident (geometrical optics) wave, u^g, and the diffracted wave, u^d, that originated at the edge of the diffracting object. This partitioning of the formula is known as the Maggi-Rubinowicz representation of the diffraction integral [Miy62a], [Miy62b], [Rub24]. It served as confirmation of Young's ideas in mathematical format. The result was generalized by Miyamoto and Wolf [Miy62a], [Miy62b] in the form:[Cro94]

$$u(P) = u^g(P) + u^d(P) \qquad \textbf{(8)}$$

where

$u^g(P) = 0$ when P lies in the shadow region

$u^g(P) = \dfrac{e^{-jkR}}{R}$ when P lies in the lit region.

and

$$u^d(P) = \frac{1}{4\pi} \oint_{\Gamma} \frac{e^{-jk(r_1+s_1)}}{r_1 s_1} \frac{\cos(n, s_1)}{1+\cos(s_1, r_1)} \sin(r_1, d\ell) d\ell \qquad \textbf{(9)}$$

where r_1 and s_1 are the distances of the point source P_0, and the observation point P, from the element $d\ell$ on the aperture contour Γ, respectively, and n is the normal to the screen aperture.

Rubinowicz made an approximation to the above expression for the diffracted field. He used the method of stationary phase [Tho87], which is valid in the high frequency approximation, and noted that only some points on the contour, Γ, of the screen contribute significantly to the scattered wave. Joseph Keller would later use this in the development of the Geometrical Theory of Diffraction. [Cro94]

In 1953, Keller developed the Geometrical Theory of Diffraction [Kel62], which has enjoyed remarkable success in the engineering community. Its application to antenna engineering has "transformed antenna design from mostly art to mostly engineering." [Han81] It has also been widely used in the prediction of diffraction in microwave radio systems, among other applications.

Keller applied a modified Fermat's principle and observed that high frequency diffraction is a local phenomenon. In doing so, he reduced the solution of the scattering of electromagnetic waves from arbitrarily shaped objects to a superposition of simple canonical problems. [Cro94].

Keller developed the theory as follows [Kel62]:
Using similar principles to Geometrical Optics:

- Assign a field value to each ray
- Total field at a point is the sum of the ray fields
- Phase of a ray is proportional to the optical length from a zero phase reference point

This procedure is used on each diffracted ray. A "diffraction coefficient" is used to adjust the value of the incident field and arrive at the initial value of the diffracted ray's field strength. The diffraction coefficient is simply multiplied by the incident field value. This is permitted since diffraction is a local phenomenon. A few notes about the diffraction coefficient are in order:

- Since diffraction is a local phenomenon, only the immediate vicinity of the point of diffraction affects the value of the diffraction coefficient. Factors affecting the

coefficients are directions of incidence and diffraction, wavelength, and geometrical and physical properties of the media. Therefore, one can use simpler, canonical problems to determine the diffraction coefficients. For more complex problems, the concept of superposition can be applied.

- As $\lambda \rightarrow 0$, the diffraction coefficients tend toward zero, as does the diffracted field. In this case, only the geometrical optics field remains.

To understand edge-diffracted rays, Keller states the following:

- Usual geometrical optics laws do not specify what happens when rays hit edges or vertices.
- These rays result in diffracted rays just as Thomas Young had predicted their existence.
- Keller concurs with Sommerfeld's suggestion that rays normally incident on an edge give rise to cylindrical waves and Keller adds that if the rays are obliquely incident on the edge, the diffracted wave in Sommerfeld's solution is conical.

To calculate the field, u_e ,on a ray diffracted by an edge, Keller makes the following points:

- Let r be the distance from the edge and the propagation constant, k = $\frac{2\pi}{\lambda}$
- The phase of the diffracted ray is $\psi_i + kr$ where ψ_i is the phase of the incident ray at the edge.
- To calculate the amplitude (considered to be a scalar):
    - Consider two neighboring rays in the same plane normal to the edge to be a tube of rays. (actually a cylinder of unit height)
    - Note that the cross sectional area of the tube is proportional to r
    - Note that the flux through the tube is proportional to rA^2
    - Since the flux must be constant, the amplitude, $A(r) \propto r^{-½}$
    - The amplitude is proportional to the incident amplitude, A_i at the edge
    - Therefore: $A(r) = DA_i r^{-½}$ where D is the diffraction coefficient

- Therefore, the edge diffracted field is

$$u_e = DA_i r^{-½} e^{j(kr+\psi i)} = Du_i r^{-½} e^{jkr} \quad \textbf{(10)}$$

where u_i is the field incident on the edge.

Now to calculate the diffraction coefficient:

- Asymptotically expand Sommerfeld's solution for large values of *kr* (i.e. "far" from the edge and/or small λ
- Compare Sommerfeld's just-expanded solution to the expression for the diffracted field.
- Sommerfeld's solution is identical if the diffraction coefficient, D, is

$$D = -\frac{e^{j\frac{\pi}{4}}}{2(2\pi k)^{\frac{1}{2}} \sin\beta}\left[\sec\frac{1}{2}(\theta-\alpha) \pm \csc\frac{1}{2}(\theta+\alpha)\right] \quad \textbf{(11)}$$

where β is the angle between the incident ray and the edge. The angles between the incident and diffracted rays and the normal to the screen are θ and α respectively. See Figure 4. The upper sign applies when the boundary condition on the half-plane is u=0, while the lower sign applies if it is $\frac{\partial u}{\partial n} = 0$.

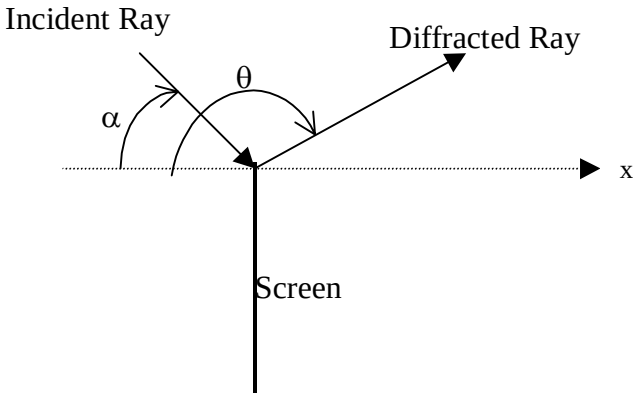

Figure 4 Projection of incident and diffracted rays into a plane normal to the edge of a screen. The edge is normal to the plane of the figure [Kel62]

In [Kel62], Keller later considers the case where the half plane is replaced by a wedge of angle (2-n)π. He follows the same procedure as above, finally comparing his expression for the diffracted field with that of Sommerfeld's exact solution for a wedge. He finds the diffraction coefficient that makes the two solutions equivalent:

$$D = \frac{e^{j\frac{\pi}{4}} \sin\frac{\pi}{n}}{n(2\pi k)^{\frac{1}{2}} \sin\beta}\left[\left(\cos\frac{\pi}{n} - \cos\frac{\theta-\alpha}{n}\right)^{-1} \mp \left(\cos\frac{\pi}{n} - \cos\frac{\theta+\alpha+\pi}{n}\right)^{-1}\right] \quad \textbf{(12)}$$

The wedge becomes a half plane for n=2 and the expression for the diffraction coefficient reduces to Equation 11.

We note that the solutions obtained by Keller are scalar. In general, a vector solution would seem to be more appropriate. As the case of high frequency solutions described in this thesis, this is not absolutely necessary. As stated in [Rus92], we are concerned about the effect of polarization on diffraction loss. Fortunately, researchers have already found that diffraction losses are not highly dependent on polarization [Lue84] and that the effects are minimal at distances greater than 50λ from the diffracting body (approximately ½ meter at 28 GHz). [Neu58].

As might be expected, there have been enhancements to the GTD since its inception. The following section presents a brief overview of some of the improvements.

In [Kou74], Kouyoumjian and Pathak develop a solution that is continuous across the shadow and reflection boundaries. This is an area where Keller's solution previously failed. The solution is again a high frequency solution, which means that diffraction can be taken as a local phenomenon. This in turn allows one to "approximate an edge geometry by a wedge whose surfaces are tangent to the surfaces forming the edge at the point of diffraction." [Kou74] The solution is obtained by adjusting the diffraction coefficients so that they are valid in the transition regions. The authors accomplished this by using "transition functions" or correction factors that are included with the diffraction coefficient. The effect of the transition functions appears in the argument of the included

Fresnel integral. The solutions presented in [Kou74] are restricted to the case of surfaces that are smooth and perfectly conducting.

In 1984, [Lue84] another enhancement to the GTD was published, this time to include finite conductivity and local surface roughness effects. This method is an extension of the GTD wedge diffraction and is again based on Fresnel integrals. Luebbers reports a minor sacrifice in terms of computational complexity with this method. He reports that by including these effects, there are two major improvements in the prediction of diffraction loss. The first improvement over the perfect conductivity, smooth surface case is that there is now little difference between the parallel and perpendicular polarization cases especially at the "higher frequencies" (10 GHz in [Lue84]). This is observed in the measurements as well. The second improvement is that the Luebbers model has a much smaller and more realistic prediction of the null depths in the interference region above the reflection boundary. He attributes this to the reduction in amplitude of reflections from the rough wedge surface. The author adds that this method can be extended to the three-dimensional predictions and multiple ridge case since it is in the context of the GTD.

3. Diffraction Measurement Description

This chapter discusses the methods and equipment used to collect the diffraction loss data. It covers goals of the measurement campaign and reviews the measurement layout and procedure. The chapter closes with a description of the test equipment and establishes its limits of operation.

3.1. Measurement Campaign Goal

The goal of the measurement campaign was to characterize additional attenuation introduced when a 28 GHz radio wave bends around an object ("diffraction"). Specifically, these diffraction losses around 90° building corners are characterized as a function of diffraction angle (θ_d) and building material. The measurements were conducted with two different polarizations: first with both antennas horizontally polarized, then with the antennas vertically polarized. These two configurations represent the "perpendicular" and "parallel" polarization states (relative to the vertical diffracting edge).

3.2. Experiment Design

This section describes the measurement layout and procedures.

3.2.1. Measurement Layout

Figure 5 below depicts the measurement layout. Note that the transmitter remains fixed in location throughout the diffraction measurements. The transmitter-corner path forms a 45° angle with the building wall. The receiver system's initial position was along the "shadow boundary" (θ_d=0°). The receiver system was then moved along an arc of constant radius taking measurement readings as the receiver moved into the shadow of

the building. Total path lengths ($r = r_i + r_d$) ranged from 39 – 50 meters. These paths lengths are clearly in the far field of the antennas. Details are shown in Table 2.

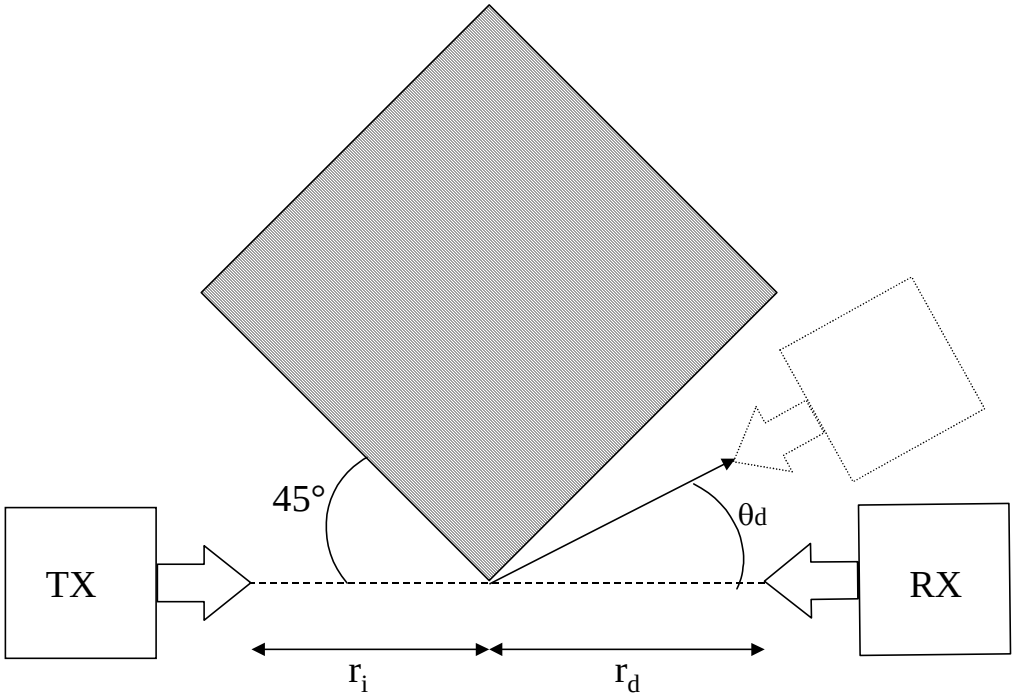

Figure 5 Diffraction measurement setup

Table 2 Diffraction measurement path lengths

Building	r_i	r_d	$r = r_i + r_d$
Building #1	20.9 m	18.2 m	39.1 m
Building #2	19.8 m	28.0 m	47.8 m
Building #3	25.0 m	25.0 m	50.0 m

The measurements reported here were made at three separate buildings in the McLean, Virginia area, a Washington, DC suburb. The tests were conducted during December 1997 and January 1998. Weather conditions were clear to partly sunny skies with temperatures ranging from 0°C to 7°C. Measurements were cancelled when windy conditions caused too much fluctuation of the measurement readings. We presumed that the fluctuations were due to the movement of the antennas in the wind.

The following is a description of the test sites:

- Building #1: Brick office building seven stories high. Building corner was sharp and formed a 90° angle. The ground surface was flat asphalt.
- Building #2: Concrete block recreation center three stories high. Building corner was sharp and formed 90° angle. The ground surface between the transmitter and diffracting corner was flat asphalt while the surface between the corner and receiver was a slight incline of grassy turf. Antenna heights, positions, and alignments were adjusted before each measurement point to ensure that the difference in antenna heights did not corrupt the results.
- Building #3: Brick school building two stories high. Building corner was sharp and formed a 90° angle. The ground surface was flat asphalt.

3.2.2.Measurement Procedure

3.2.2.1. Test site selection

Selected test sites were generally level surfaces clear of obstructions nearby the diffracting corner, in or adjacent to the propagation path.

3.2.2.2. Methodology

- A clear line of sight measurement was made over a path length and ground conditions that were the same as the diffracted path.
- The diffraction measurements were made by starting with the receiver, diffracting corner, and transmitter in a straight line (along the shadow boundary). The transmitter and receiver antennas were pointing at each other. The transmitter remains fixed in location throughout the diffraction measurements.
- Starting from 0° diffraction angle (θ_d), the receiver system was moved along an arc of constant radius taking measurement readings as the receiver moved into the shadow of the building.

- The antenna positions were adjusted before each measurement point to ensure maximum received signal via the diffraction path.
- Measurements were taken at diffraction angles (θ_d) ranging from 0° to 45°.
- Each test site was tested two times: once with both antennas (linearly) polarized perpendicular to the diffracting edge ($\perp$) and once with the antennas polarized parallel to the edge($\parallel$).
- Isolating the effect of the diffraction propagation mechanism was of primary importance. Care was taken not to allow any unwanted propagation paths (ground reflections, etc.), spurious radio sources, or weather conditions to corrupt the results. To identify unwanted propagation paths, we moved an obstruction around the sides of the receive antenna and watched for received signal fluctuation. The test area was scanned before measurements to ensure the were no other transmitters operating at 28 GHz. Measurements were made under clear skies.
- The diffracted received signal strength was compared to the line of sight measurement. The difference between the two signal levels was taken to be the excess loss due to the diffracting corner (*E*).

3.3. Test Equipment Specifications

This section discusses the parameters that govern the operation of the test equipment. It begins with an overall view of the system.

3.3.1. Test Equipment Configuration

The measurement system consisted of a transmitter and receiver system. The block diagram shows the transmitter system configuration.

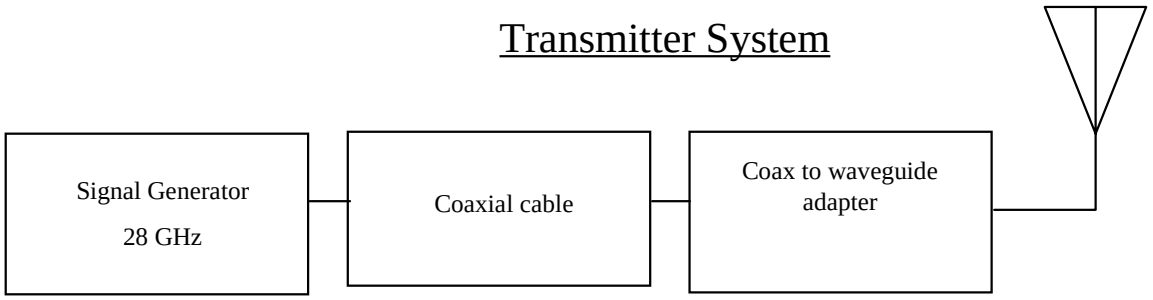

Figure 6 Transmitter system block diagram

The Hewlett Packard HP 83640B signal generator produced the test signal. It was used to generate a 28.0 GHz continuous wave (CW) signal. This unit was suitable on account of its portability, ruggedness and wide operating temperature range. The coaxial cable used to transport the signal between components is a high frequency UTiFLEX® 2.4 mm cable. The transmit antenna was a parabolic antenna by Gabriel Electronics with a 2.5° beamwidth and 36 dBi gain. The narrow beam of the antenna allowed for precise pointing and enabled the signal to be focused on a small area. The antenna was mounted on a tripod that allowed motion in all three planes.

The receiver system configuration is shown in the block diagram below.

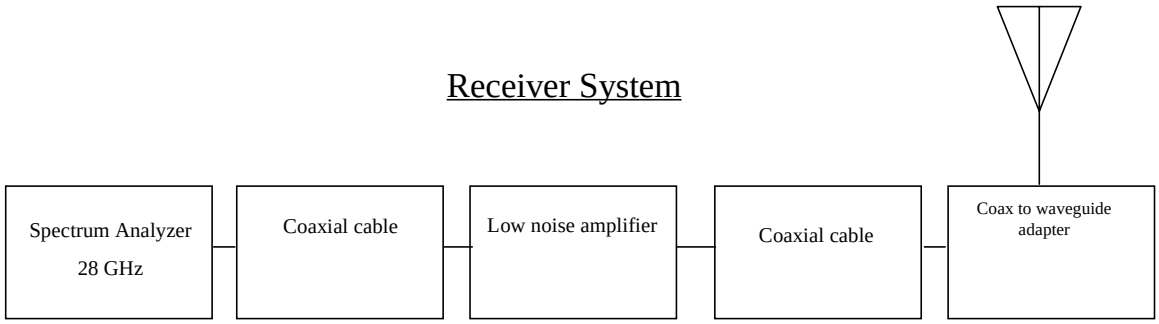

Figure 7 Receiver system block diagram

The receive antenna is a horn made by Flam & Russell with a beamwidth of 17° and a 16 dBi gain. This antenna was appropriate due to its wider beam which would ease the task of finding the transmitted “pencil” beam. At the same time, the antenna had a beam that

was narrow enough to reject unwanted signals. This antenna was mounted on a tripod that allowed motion in all three planes. The coaxial cable used to transport the signal between components is a high frequency UTiFLEX® 2.4 mm cable. A wideband low noise amplifier was used to boost the signal on the receive side. This HP 83050A amplifier has a very broad frequency range (2-50 GHz) and has a reasonable noise figure of 10 dB for such a wide range of operating frequencies. Its small weight (640 grams) and footprint simplified mounting of the amplifier on the tripod. The Hewlett Packard HP 8546E portable spectrum analyzer was used as the test receiver and measurement device. Like the HP signal generator, this unit was also suitable on account of its portability, ruggedness and wide operating temperature range

3.3.2.System Calculations

The following sections examine factors that limit the performance of the measurement system. First, the noise budget will be calculated followed by a signal or "power budget".

3.3.2.1. Noise budget

This section calculates the minimum detectable signal. Since there were few other terrestrial users in the 28 GHz band, the lower bound on measurement system sensitivity is a function of ambient and system noise. Since the impedances in this communication system are matched (at 50 ohms), the noise figures of the attenuators are simply the reciprocal of the gain. This will simplify the calculations. Table 3 and Figure 8 summarize the relevant receiver system parameters and are followed by the noise calculations.

Table 3 Receiver system noise budget parameters

Component	Loss Linear (*dB*)	Gain (G) Linear (*dB*)	Noise Figure (F) Linear (*dB*)	Symbol
Coaxial Cable (2') [Uti97]	1.39 (*1.44*)	0.718 (*-1.44*)	1.39 (*1.44*)	G_1 and F_1
LNA [Hew97e]		125.9 (*21*)	10 (*10*)	G_2 and F_2
Coaxial Cable (10')[Uti97]	5.25 (*7.2*)	0.191 (*-7.2*)	5.25 (*7.2*)	G_3 and F_3
Spectrum Analyzer			3162 (*35*)	F_4

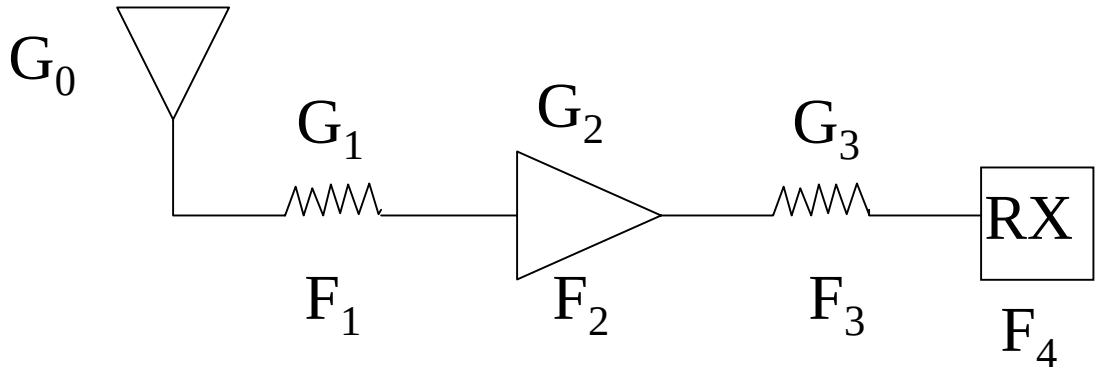

Figure 8 Noise Block Diagram

3.3.2.1.1. Spectrum Analyzer noise figure calculation:

Displayed average noise level =< -139 dBm (1 Hz resolution bandwidth) [Hew97a]

Thermal noise in 1 Hz bandwidth = kTB = (1.38 E-23) * (290) * (1) = -174 dBm

Therefore maximum noise due to spectrum analyzer = -139 dBm - (-174 dBm)

$$\mathbf{F_{SA,\,MAX} = 35\ dB} \qquad \textbf{(13)}$$

3.3.2.1.2. System noise figure calculation

Using the noise figure calculation for cascaded devices (at the antenna terminals) and referring to Figure 8 [Hew97b]:

$$F_{SYS,\,ANT} = F_1 + (F_2-1)/G_1 + (F_3-1)/(G_1G_2) + (F_4-1)/(G_1G_2G_3) + \ldots \text{[Mum68]} \quad \textbf{(14)}$$

$$= 1.39 + (10-1)/(0.718) + (5.25-1)/(0.718*125.9) + (3162-1)/(0.718*125.9*0.191)$$

$$\underline{\mathbf{F_{SYS,\,ANT} = 197 = 23\ dB}} \quad \textbf{(15)}$$

3.3.2.1.3. System Noise temperature calculation

The system noise temperature at the antenna terminals is:

$$T_{SYS,\,ANT} = T_0\,(F_{SYS,\,ANT} - 1) = 290 * (197 - 1)\ \text{[Vir97]} \quad \textbf{(16)}$$

$$\underline{\mathbf{T_{SYS,\,ANT} = 56840\ K}} \quad \textbf{(17)}$$

Since this value is very large relative to the antenna temperature, T_{ANT} will be neglected.

4) Noise floor calculation

We choose the resolution bandwidth (RBW) wide enough so that the frequency error in the transmitted signal is easy to locate within the RBW of the spectrum analyzer. We choose RBW = 1 kHz.

Noise floor $= kT_{SYS,\,ANT}B$

$= (1.38\ E\text{-}23) * (56840) * (1000)$

Noise floor = -121 dBm **(18)**

Allowing a 10 dB margin over the noise, we set the minimum detectable signal (MDS) at (-121 dBm) + (10 dB)

MDS = -111 dBm **(19)**

3.3.2.2. Signal Budget

The signal budget determines what transmitter powers are required so that the measurement system functions within its operational limits. These limits are imposed by the amplifier or receiver overdrive level (upper bound) and the MDS (lower bound). Depending on the distance between the transmitter and receiver, the transmitter output power may require adjustment to stay within the measurement system's operational bounds. In this section, these bounds will be calculated followed by the recommended transmitter power calculation. The relevant system parameters are shown in Table 4 and Figure 9

Table 4 System power budget parameters

Component	Gain (G)	Symbol	$P_{OUT, MAX}$ (dBm)	1 dB compression point (dBm)	$P_{IN, MAX}$ (dBm)
Receive Antenna [Gab]	36.1 dBi	G_0			
Coaxial Cable (2') [Uti97]	-1.44 dB	L_1			
LNA [Hew97e]	21 dB	G_2		15	
Coaxial Cable (10')[Uti97]	-7.2 dB	L_3, L_5			
Spectrum Analyzer [Hew97b]		F_4			30
Signal Generator [Hew97c]		TX	+6		
Coax/waveguide adapter [Hew97g], [Mic]	Negligible				
Transmit Antenna [Fla95]	17 dBi	G_6			

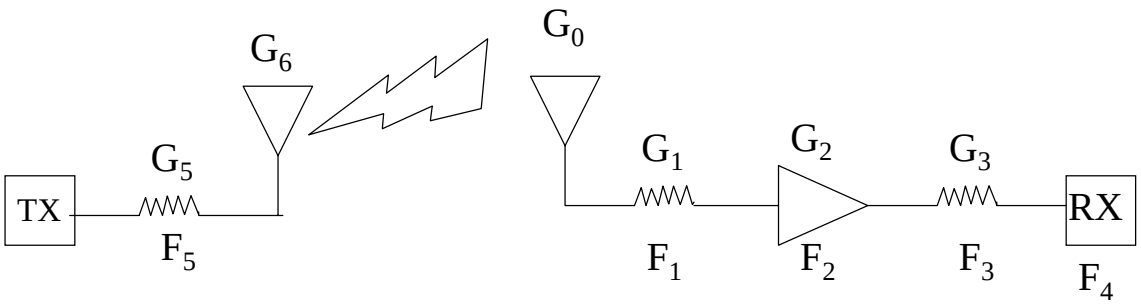

Figure 9 Signal Block Diagram

3.3.2.2.1. Lower operational bound

In order for the measurement system to accurately measure the received signal, the signal level at the receiver front end must be stronger than the minimum detectable signal (MDS) of -111 dBm. The link budget is then:

MDS <= Signal at receiver front end

$$MDS <= P_{TX} - L_5 + G_6 - L_{POINTING} - FSL - L_{PATH} + G_0 - L_1 + G_2 - L_3$$

where FSL = free space loss = $92.45 + 20 \log f_{GHz} + 20 \log d_{km}$ **(20)**

Rearranging:

$$MDS + L_5 + L_{POINTING} - G_0 - G_2 + L_1 + L_3 - G_6 <= P_{TX} - FSL - L_{PATH}$$

Substituting fixed values:

-111 dBm + 7.2 dB + 0.5 dB -17 dBi - 21 dB + 1.44 dB + 7.2 dB - 36.1 dBi

$<= P_{TX} - FSL - L_{PATH}$

Therefore,

Lower operational bound is: $FSL + L_{PATH} - P_{TX} <= 168.8$ dB **(21)**

3.3.2.2.2. Upper operational bound

In order for the measurement system to accurately measure the received signal, the signal level at the receiver front end must be weaker than the rated maximum power in. Also, the signal into the amplifier must not drive the amplifier into compression. We will employ the link budget to calculate the upper operational bound for both of these cases.

3.3.2.2.2.1. Upper bound based on amplifier compression

The amplifier 1 dB compression point (P_1) is the power level "which the amplifier generates when driven by an RF level that is sufficient [strong enough] to compress [its gain] 1 dB from its small signal value" [Vir97]. Expanding the link budget from transmitter to amplifier and constraining the amplifier input signal to be less than P_1:

$$P_{TX} - L_5 + G_6 - L_{POINTING} - FSL - L_{PATH} + G_0 - L_1 + G_2 <= P_1 \quad \textbf{(22)}$$

Rearranging:

$$P_{TX} - FSL - L_{PATH} <= P_1 + L_5 - G_6 + L_{POINTING} - G_0 + L_1 - G_2$$

$$P_{TX} - FSL - L_{PATH} <= 15 \text{ dBm} + 7.2 \text{ dB} - 17 \text{ dBi} + 0.5 \text{ dB} - 36.1 \text{ dBi} + 1.44 \text{ dB} - 21 \text{ dB}$$

$$P_{TX} - FSL - L_{PATH} <= -50 \text{ dB}$$

Therefore,

Upper operational bound due to amplifier compression is: $FSL + L_{PATH} - P_{TX} >= 50.0$ dB **(23)**

3.3.2.2.2.2. Upper bound based on spectrum analyzer power rating

In order to measure accurately and to avoid damage to the spectrum analyzer, the power into this device must be below the rated maximum. Examining the link budget:

$P_{IN, MAX}$ >= Power into spectrum analyzer

$$P_{IN, MAX} >= P_{TX} - L_3 + G_4 - L_{POINTING} - FSL - L_{PATH} + G_0 - L_1 + G_2 - L_3 \quad \textbf{(24)}$$

Rearranging:

$$P_{IN, MAX} + L_3 - G_4 + L_{POINTING} - G_0 + L_1 - G_2 + L_3 >= P_{TX} - FSL - L_{PATH}$$

Substituting values:

30 dBm + 7.2 dB - 36.1 dBi + 0.5 dB - 17 dBi + 1.44 dB - 21 dB + 7.2 dB

$$>= P_{TX} - FSL - L_{PATH}$$

$$P_{TX} - FSL - L_{PATH} <= -27.8 \text{ dB} \quad \textbf{(25)}$$

Therefore

Upper operational bound due to spectrum analyzer limit is: $FSL + L_{PATH} - P_{TX} >= 27.8$ dB

Since the amplifier compression imposes a stricter upper bound, we conclude:

Upper operational bound is: $FSL + L_{PATH} - P_{TX} >= 50.0$ dB **(26)**

3.3.2.2.3. Selection of transmitter power

Now that the operational bounds of the measurement system have been defined, we can select transmitter power ranges that are appropriate for each measurement case. Recalling the two bounds:

Upper operational bound is: FSL + L_{PATH} - P_{TX} >= 50.0 dB

Lower operational bound is: FSL + L_{PATH} -P_{TX} <= 168.8 dB

We note that the bounds depend on transmitter power, free space loss and diffraction loss. In all tests, we will attempt to stay away from the bounds of operation. Appropriate transmitter powers will now be discussed.

Both the FSL and diffraction losses are substantial and must be considered. The expected range of path lengths is given in Table 5 as well as a liberal allowance for diffraction losses. [Vio88]

Table 5 Free space and diffraction loss allowances

Path length	FSL	Diffraction loss	Total Loss
6 - 53 meters	77 - 96 dB	0 - 75 dB	77- 171 dB

In order to operate within the lower bound (FSL + L_{PATH} -P_{TX} <= 168.8 dB), P_{TX} >= +2 dBm. Since the lower bound is of greatest concern in this case, it would be prudent to choose the maximum specified transmitter power of +6 dBm. Therefore,

P_{TX} ≅ +6 dBm ∀ diffraction measurements; r =(6 m,53 m)

At +6 dBm transmitter power, the system has 97 dB of dynamic range.

3.4. Summary

This chapter has detailed the methods and equipment used to collect the diffraction loss data. Measurement layout and procedures were covered as well as a presentation of the test equipment and its limits of operation. The next section presents and discusses the measurement results.

4. Measurement Results and Interpretation

This chapter presents, discusses, and characterizes the measurement results. First, is a general introduction to the results, followed by a presentation of the data as measured. Next, is a discussion of trends noted in the results. Finally, there is a presentation of a mathematical model that describes the measured data.

As expected, the measurements showed an increasing attenuation as the receiver moved in the shadow of the building (as the diffraction angle increased). In general, the diffraction loss measurements were very consistent at each diffraction angle for all tests, indicating a high degree of consistency in the results. There were two anomalies worth mentioning, though. When $\theta_d = 45°$, the measurement results were highly variable. This angle corresponds to the tripod being placed against the wall with the antenna pointing along the length of the wall (refer to Figure 5). Positioning of the antenna at this angle was very difficult and is most likely the cause of the larger measurement variability at this angle. Therefore, the data at $\theta_d = 45°$ was not considered in the analysis. The other anomaly in the measurement results occurred on a LOS measurement on building #2 which was approximately 5.5 dB different from other LOS measurements for equivalent path lengths. The data point was not re-measured at the time and is considered an outlier. Therefore, this LOS data point was set equal to the LOS measurement made over the same path but with opposite polarization. A presentation of the data as measured follows.

4.1. Measurement Data

Figure 10, Figure 11, and Figure 12 depict the excess loss (*E*) due to the diffracting corner as a function of diffraction angle, θ_d. The quantity *E*, expressed in dB, is the difference between the free space loss (see page 28) and the loss experienced over the diffraction path. This is the quantity normally calculated in analyses of diffraction and the subject of

this thesis. To review the measurement layout, see Figure 5. Note that there are two sets of measurements for each building corner: antennas horizontally polarized ("H-H" or perpendicular to the diffracting edge) and antennas vertically polarized ("V-V", or parallel to the diffracting edge). The section that follows begins the evaluation by reviewing trends or dependencies in the data.

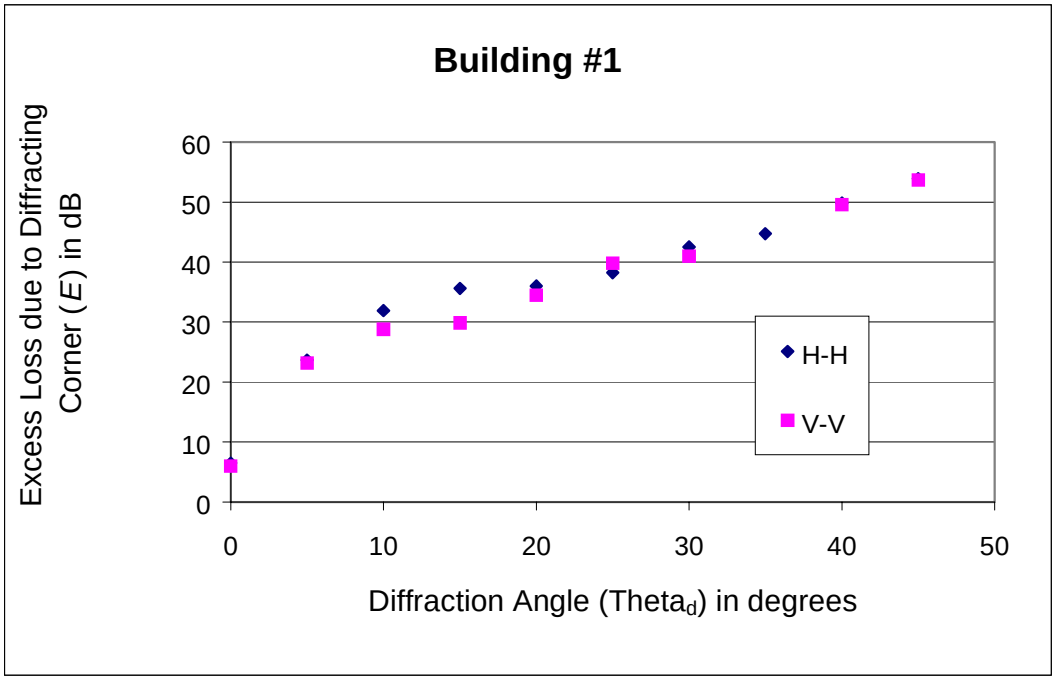

Figure 10 Excess loss due to diffracting corner , Building #1

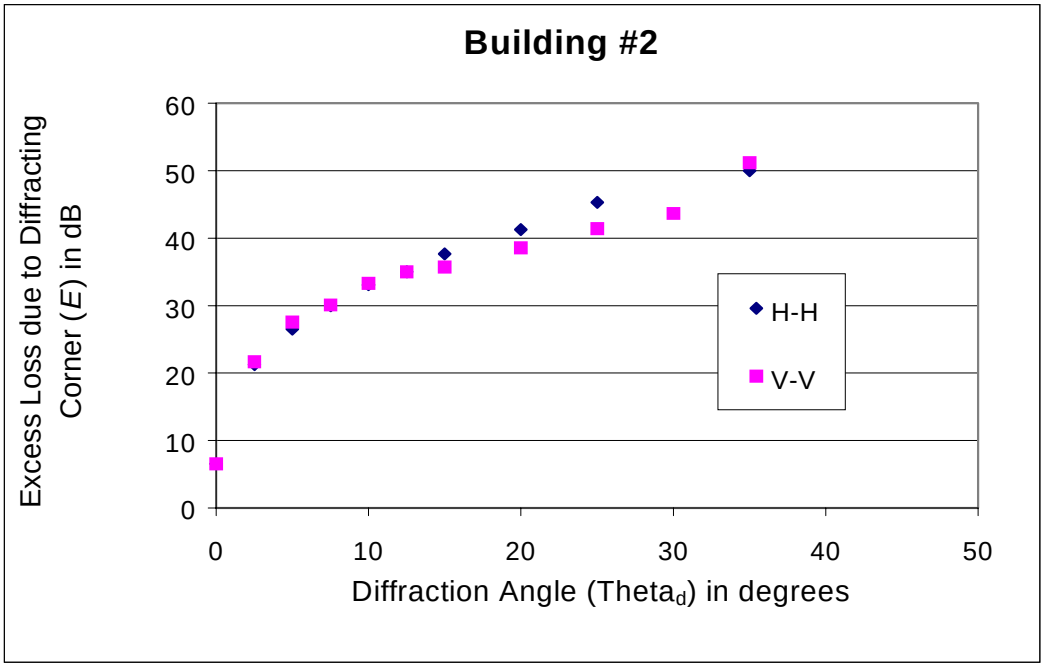

Figure 11 Excess loss due to diffracting corner, Building #2

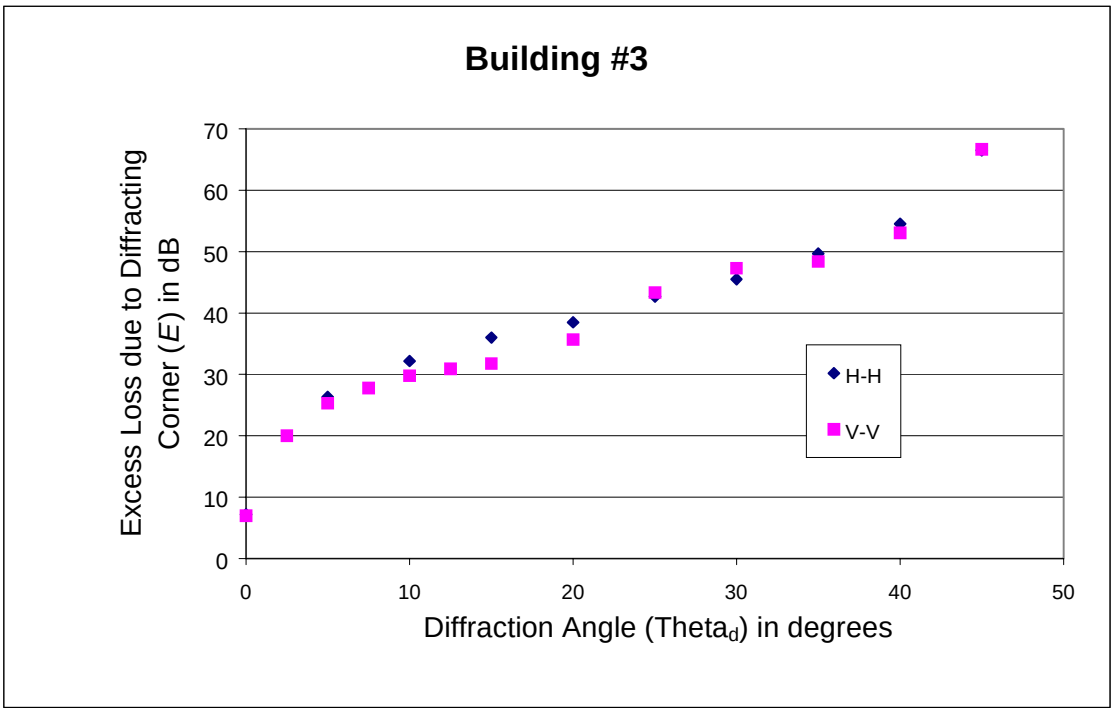

Figure 12 Excess loss due to diffracting corner, Building #3

4.2. Measurement Trends

This section discusses the following dependencies in the measurement results:

- Diffraction Angle
- Building Material
- Polarization
- Path Length and Geometry

4.2.1.Diffraction Angle

The diffraction angle was the key variable in the characterization of the excess loss, *E*. The losses increased approximately linearly with increasing angle (dB loss vs. angle) for angles 5° and greater. For angles smaller than 5°, the attenuation grew more rapidly with angle and exhibited a logarithmic growth. At the 0° diffraction angle, losses ranged from 6-7 dB. Since there are two distinctly different behaviors at large and small angles, the mathematical model developed later is piecewise.

Figure 13 shows all the excess loss data on one graph. The logarithmic and linear relations are clearly visible. The different symbols indicate the different test cases (building and polarization).

Figure 13 Diffraction angle vs. excess loss

4.2.2.Building Material

The dependence on building material was small but noticeable. The results are shown in Figure 14. The rougher concrete block corner attenuated the signal by about 3 dB more than the brick corner across diffraction angles from 5° to 40°. This result is expected since the corner roughness approaches the wavelength at 28 GHz. This causes more incident energy to be scattered diffusely when it impinges on the edge and wall. Luebbers [Lue84] noted this when he studied the GTD for the finite conductivity case. At small angles, where the LOS component is still strong, the losses are approximately equal.

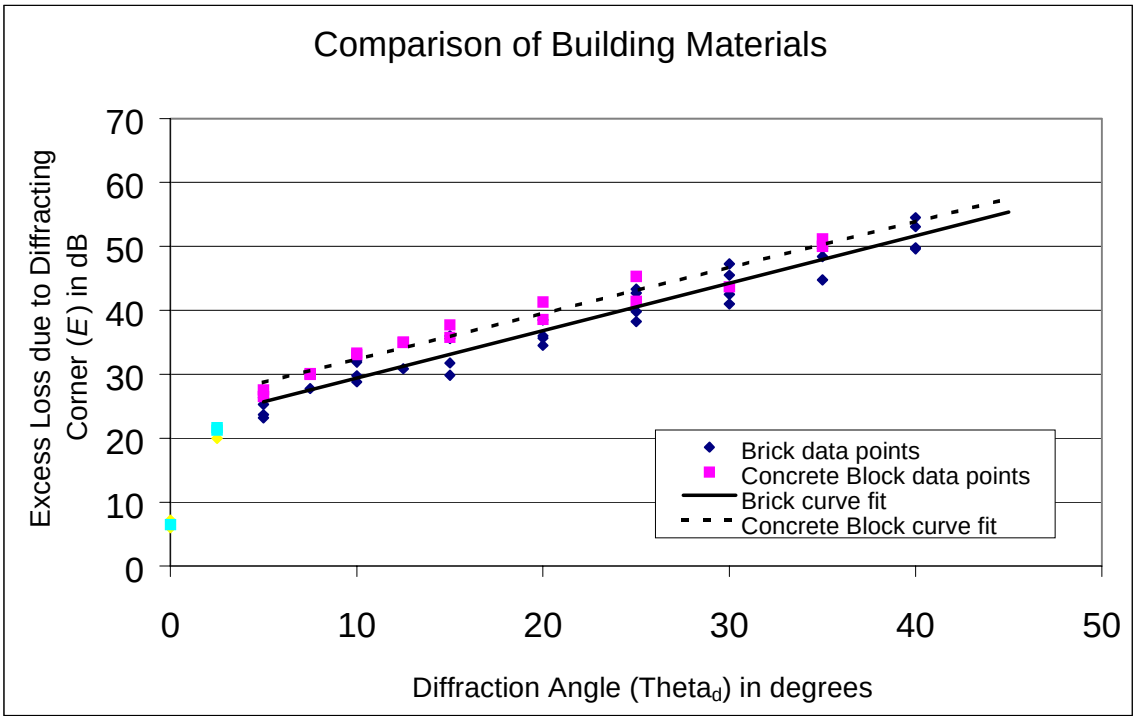

Figure 14 Excess loss for different building materials

4.2.3.Polarization

The dependence on polarization was weak, with less than 1.5 dB difference between the two linear polarizations. See Figure 15. At small angles, the excess losses were virtually identical.

These results agrees other measurements including [Lue84] where polarization played a minor role in diffraction losses, especially at high frequencies.

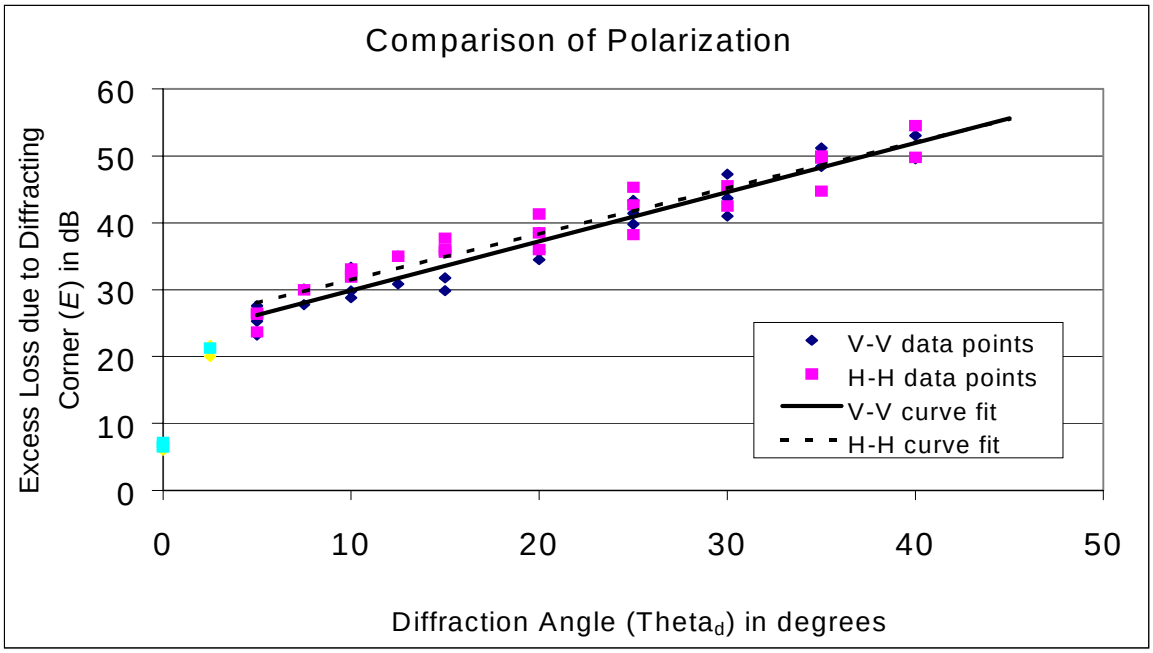

Figure 15 Excess loss for different polarizations

4.2.4.Path Length and Geometry

This section will examine the impact of path length and geometry. The first subsection addresses path length.

4.2.4.1. Path Length

There was no apparent dependence on path length. The excess loss curves were similar all three path geometries. We examine the mathematical expression for excess path loss:

$$E = \frac{S_F}{S_D} \tag{27}$$

where S_F and S_D are the signal level on the free space and diffracted paths, respectively. (See Figure 5). Their expressions are

$$S_F \propto (r^2)^{-1} \tag{28}$$

and

$$S_D \propto (r_i^2 \, r_d^2 \, L_d)^{-1} \qquad \textbf{(29)}$$

where

$$r = r_i + r_d. \qquad \textbf{(30)}$$

Diffraction loss, L_d, is a quantity introduced in the mathematical modeling of diffraction. Combining these two equations, we find that

$$E = \frac{S_F}{S_D} = L_d\left[\frac{1}{r_d}+\frac{1}{r_i}\right]^2 = L_d \text{ (dB)} - 20 \log \left[\frac{1}{r_d}+\frac{1}{r_i}\right] \qquad \textbf{(31)}$$

Thus $E = 20\log\left(\frac{S_F}{S_D}\right)$ depends on path length if L_d is constant. E is not equal to the dB value of L_d and E should not be equated with L_d. Both experimental evidence [Vio88] and analyses of knife edge diffraction [Gri87] indicate that E is independent of path length. This implies that L_d is not constant or that the equations used for S_F and S_D are incorrect. We do not address the issue of which of these conditions is true since this thesis is concerned with E rather than with L_d.

4.2.4.2. Path Geometry

This section addresses the question of "How does E depend on path geometry?" Let's assume L_d is constant. In the measurements discussed here, the diffracting corner is approximately at the center of the path and $r_i = r_d$. We will call such a path a symmetric path. A path where r_i is not equal to r_d is an asymmetric path. How much difference does path asymmetry make?

In most practical situations, the diffracting corner will be far from one end of the radio path and close to the other end. We will represent this situation by assuming that $r_d >> r_i$. Under these conditions r_d will have little effect on *E*. See the values tabulated in Table 6. The difference in *E* between a path where $r_d = r_i = 25$m and paths in which $r_d > 1000$m and $r_i = 25$m is only about 6 dB and this is comparable to the variation in measurements between different buildings. Thus our measurements for paths with $r_d = r_i = 25$m would seem to be applicable to many practical paths.

Table 6 Path geometry dependence

R_i (m)	R_d (m)	20 log $\left[\frac{1}{rd}+\frac{1}{ri}\right]$ term (dB)
25	25	21.94
1000	25	27.94
5000	25	27.92
10000	25	27.94

After examining the trends in the measurement results, we developed a mathematical model to characterize the diffraction losses.

4.3. Simplified Mathematical Model

Since the measurement values at each measurement angle were closely clustered, it made sense to put all of the measurement points together and develop a single model. Due to the difference in behavior at small and large angles, this model is piecewise for the two regions: (0°, 5°), “small angle diffraction” and [5°, 40°], “large angle diffraction.”

4.3.1. Small angle diffraction

The small angle results are shown in Figure 16.

A curve fit to the data yielded the following:

$$E = 5\ln\theta_d + 18 \quad \text{for } 0.1° \geq \theta_d > 5° \qquad \textbf{(32)}$$

where E is the excess loss in dB (defined in section 4.1) and θ_d is the diffraction angle in degrees. The curve fit the data very well with $R^2 = 0.98$. The R^2 is a statistical measure of how well the curve represents the data where $0 \leq R^2 \leq 1$. This equation is suitable for system design predictions of 28 GHz diffraction around 90° building corners.

Note that the equation for small angles is singular at angles near the shadow boundary ($\theta_d < 0.1°$). The appropriate value to use in this case is 6.5 dB as the measurements were closely clustered about this value.

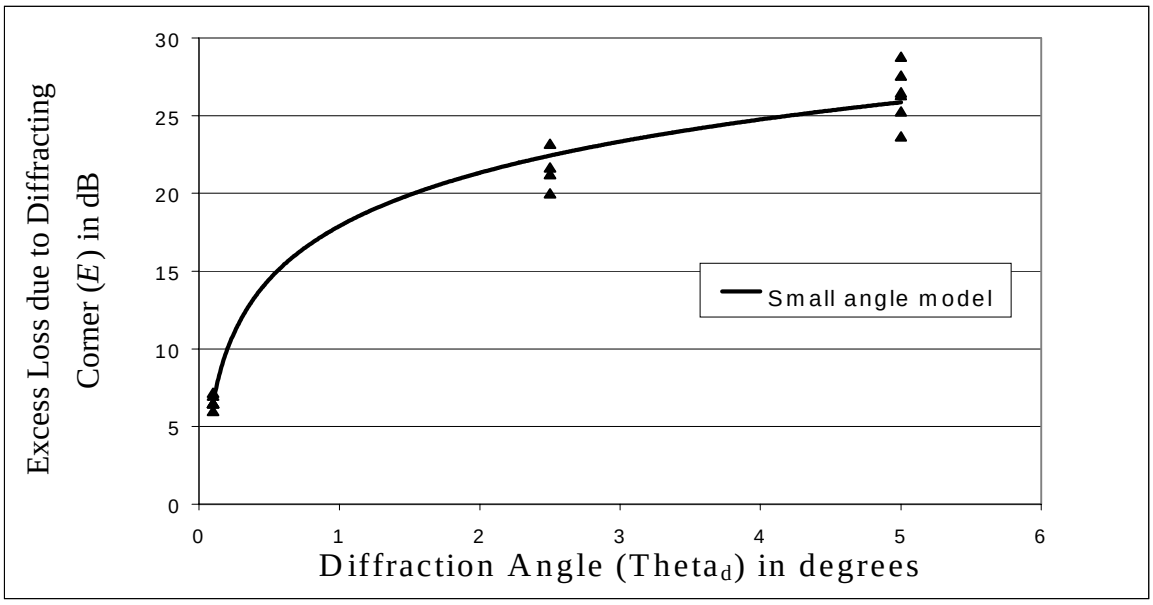

Figure 16 Small angle diffraction model

4.3.2.Large angle diffraction

The large angle results are shown in Figure 17.

A curve fit to the median values yielded the following:

$$E_{MED} = 0.684\ \theta_d + 24.6 \quad \textbf{(33)}$$

where E_{MED} is excess loss in dB (as defined in section 4.1) and θ_d is the diffraction angle in degrees. E_{MED} represents the level at which 50% of the points lie above the curve and 50% are below. The curve fit the data very well with $R^2 = 0.98$.

A more stringent criteria is the 95 % confidence level. The curve for this level is:

$$E_{95} = 0.726\ \theta_d + 25.1 \quad \textbf{(34)}$$

where E_{95} is excess loss in dB and θ_d is the diffraction angle in degrees. E_{95} represents the level where 95% of the values lie below the curve (i.e. smaller values of loss). In order to calculate the confidence interval, we assumed that the received signal is Gaussian distributed. The curve fit the data exceptionally well with $R^2 = 0.99$.

The most conservative characterization of these measurements is the upper bound, whose curve is fitted to the maximum excess loss received at each measurement angle. The equation is:

$$E_{UPPER} = 0.749\ \theta_d + 25.35 \quad \textbf{(35)}$$

where E_{UPPER} is excess loss in dB and θ_d is the diffraction angle in degrees. This represents the level where all of the measurement points lie on or below the curve. The curve fit the data exceptionally well with $R^2 = 0.99$.

The large angle behavior can be summarized in a single equation due to excellent curve fits and consistent results for all the measurements. The following equation is suitable for system design predictions of 28 GHz diffraction around 90° building corners:

$$E = 0.74\,\theta_d + 25, \quad \text{for} \quad 5° \geq \theta_d \geq 40° \qquad \textbf{(36)}$$

where E is large angle excess loss in dB (as defined in section 4.1) and θ_d is the diffraction angle in degrees

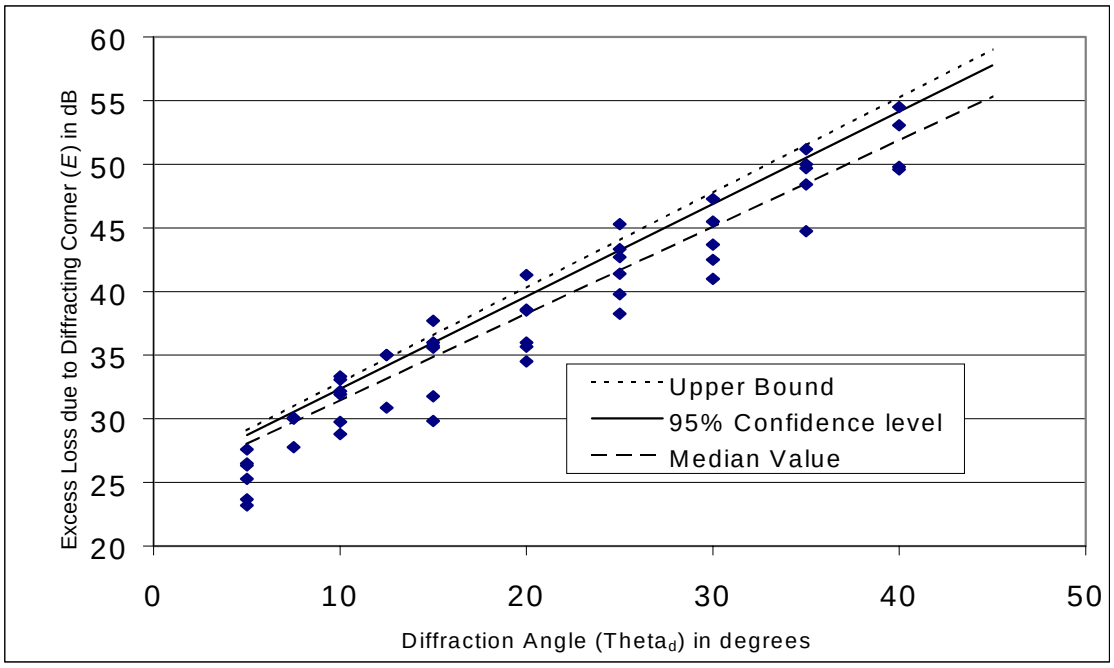

Figure 17 Large angle diffraction model

4.3.3.Mathematical model summary

Table 7 summarizes the 28 GHz, 90° building corner, mathematical model

Table 7 Building corner excess diffraction loss model

Diffraction Angle (θ_d) in degrees	Excess Loss due to Diffracting Corner (E) in dB
$0° \geq \theta_d > 0.1°$	6.5
$0.1° \geq \theta_d > 5°$	$5\ln \theta_d + 18$
$5° \geq \theta_d \geq 40°$	$0.74\ \theta_d + 25$

4.3.4.Comparison of model to theory

This simplified model in Table 7 not only compares well with the data collected, but also with the diffraction loss predicted by the GTD with a knife edge obstacle. The large angle comparison to theory is shown in Figure 18 where the predicted value is calculated on page 16. The small angle prediction is equivalent to the simplified model for diffraction angles less than five degrees. The simplified model does not contain an erroneous dependence on polarization like the GTD prediction. Note that "parallel polarization" is the case when antennas' polarization and the diffracting edge are parallel (vertical in the case of this experiment). Perpendicular polarization refers to the antenna polarizations are perpendicular to the edge. [Lue84] notes that under conditions of relatively small wedge angles and with "incident and diffracted rays are sufficiently removed from grazing", the wedge and knife edge diffraction models give "essentially identical" results. The reader should note that a 90°wedge angle is "relatively small" compared to those discussed in [Lue84].

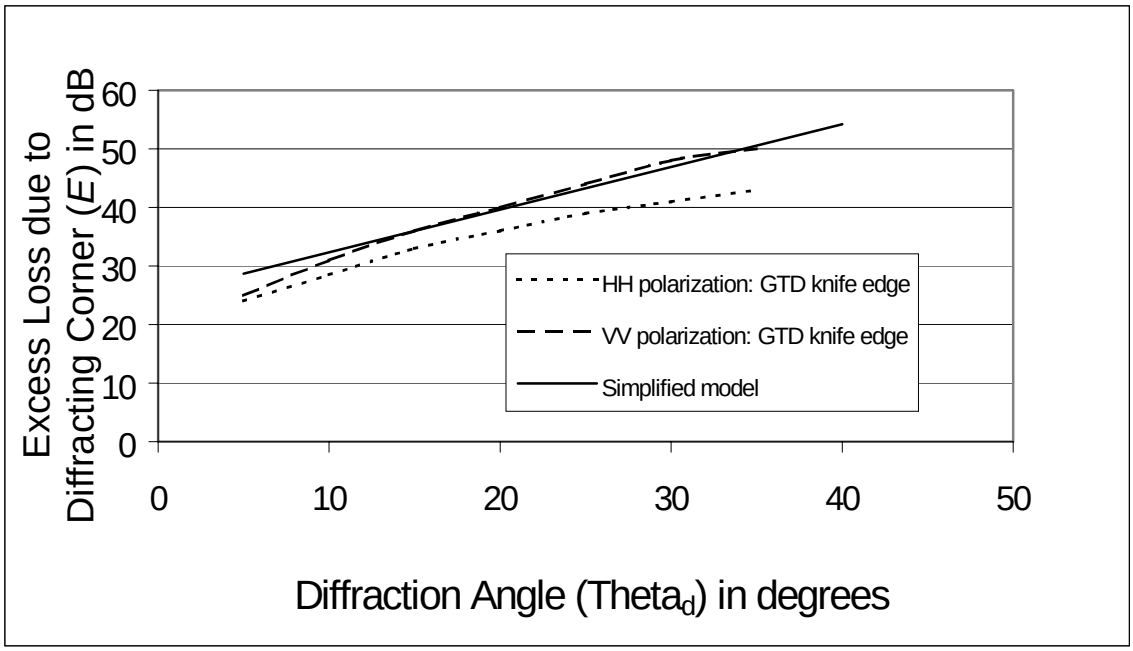

Figure 18 Simplified model vs. GTD around vertical edge

4.3.5.Comparison of model to other measurements

The trends in our measurement results are similar to previous measurements made around wedge-shaped diffracting objects including [Lue84]. The measurement results were very consistent, indicating a high level of confidence that can be placed on the results for 90° corners.

Measurements around rounded corners showed higher losses and more polarization dependence than the 90° corner case. The following are examples of this deviation:

- In Violette, et al., [Vio88], measurements around one building corner at 28.8 GHz show approximately 10 – 15 dB more loss than the GTD knife edge predictions. The deviation is somewhat smaller from our measurements. These measurements in [Vio88] were *not* made on a corner that was a sharp 90° corner. "In fact, the concrete corners are formed such that they have a 1.5 cm flat bevel at 45° to each side" [Vio88]. There was a clear polarization dependence with higher attenuation (diffraction loss) in the parallel polarization case.

- In [Neu58], there was a strong polarization dependence during Neugebauer's tests in the K-band over a scale model of cylindrical mountains. These tests were made on a small model and for only small diffraction angles.

This larger attenuation is probably due to the rounded corner shape in these measurements. Alternatively, there could have been differences in experimental procedure that gave different results.

Possible means for resolving this discrepancy and further validating the model are discussed in the next section.

4.4. Items for Further Study

In order to provide further substantiation to the model developed here, the following tests would be appropriate:

- Measure diffraction loss of other building corners that are not sharp and/or 90° corners in order to validate effect of corner geometry.
- Test several other building corners constructed from a variety of building materials (roughness) to characterize and determine the effect of roughness.
- Place the (fixed location) transmit antenna at various angles relative to the building wall and repeat the experiment to determine any impact on diffraction loss.
- Make multiple tests on same building to validate independence of diffraction loss and path length.

5. Conclusions

This thesis reviews the fixed wireless industry and it's engineering system design issues in the first chapter. It also discusses the importance of characterization of diffraction. There is a review of diffraction history and theory in Chapter 2. A description of the 28 GHz building corner diffraction measurement campaign appears in the Chapter 3. Chapter 4 identifies diffraction dependencies, develops a mathematical model, and compares the model to theory and measurements of other researchers.
The key findings in this thesis are:

- Mathematical model for 90° building corners at 28 GHz:

Diffraction Angle (degrees)	Diffraction loss (dB)	Refer to
$0° \geq \theta_d > 0.1°$	6.5	Figure 16
$0.1° \geq \theta_d > 5°$	$5\ln \theta_d + 18$	Figure 16
$5° \geq \theta_d \geq 40°$	$0.74\ \theta_d + 25$	Figure 17

- Diffraction angle dependence. The diffraction angle was the key variable in the characterization of diffraction losses. The relation between angle and diffraction loss was generally linear (dB loss vs. angle) for angles 5° and greater. For angles smaller than 5°, the attenuation grew more rapidly with angle and exhibited a logarithmic growth. At the 0° diffraction angle, losses ranged from 6-7 dB.
- Building material dependence. The dependence on building material was small but noticeable. The rougher concrete block corner attenuated the signal by 3 dB more than the brick corner across diffraction angles from 5° to 40°.
- Polarization dependence. The dependence on polarization was weak, with less than a 1.5 dB difference between the two linear polarizations.
- Path length dependence. There was no apparent dependence on path length.

The model shows close agreement with theory and measurements of other 90° corners.

In order to provide further substantiation to the model developed here, the following tests would be appropriate:

- Measure diffraction loss of several other building corners that are not sharp and/or 90° corners in order to validate effect of corner geometry.
- Test several other building corners constructed from a variety of building materials (roughness) to characterize and determine the effect of roughness.
- Place the (fixed location) transmit antenna at various angles relative to the building wall and repeat the experiment to determine any impact on diffraction loss.

6. References

[Boga] *Bogen Tripod Catalog*, Bogen Photo Corp, Ramsey, NJ, p.5.

[Bogb] *Bogen Tripod Catalog*, Bogen Photo Corp, Ramsey, NJ, p.7.

[Cro90] W.F. Croswell, R. Cecchini, and G. Pelosi, "Diffraction: The First Recorded Observation," *IEEE Antennas and Propagat. Soc. Mag.*, Vol. 32, No.2, pp. 27-30, Apr. 1990.

[Cro94] W.F. Croswell, O.M. Bucci, and G. Pelosi, "From Wave Theory to Ray Optics," *IEEE Antennas and Propagat. Mag.*, Vol. 36, No.4, pp. 35-42, Aug. 1994.

[Fla95] *Flam & Russell, Inc. Measurement Products Catalog*, Flam & Russell, Inc., Horsham, PA, 1995.

[Fre66] A.J. Fresnel, "*Oeuvrés complètes d'Augustin Fresnel*, Imprimerie Impériale, Paris, 1866.

[Gab] *Gabriel Electronics Catalog*, Gabriel Electronics, Incorporated, Scarborough, ME, p.84.

[Gri65] F.M. Grimaldi, *De Lumine*, 1665

[Gri87] J. Griffiths, *Radio Wave Propagation and Antennas*, Englewood Cliffs, NJ: Prentice-Hall, 1987.

[Han81] R.C. Hansen (ed.), *Geometrical Theory of Diffraction*, New York: IEEE Press, 1981.

[Hel73] H. Helmholtz, from *Popular Lectures*, London, p. 249, 1873.

[Hew97a] *Hewlett Packard 1997 Test and Measurement Catalog*, Santa Clara, CA, 1996, pp. 238-40.

[Hew97b] *HP 8560 E-Series Spectrum Analyzers - Technical Specifications*, via fax from Hewlett Packard Test and Measurement Call Center, Engelwood, CO, 1997.

[Hew97c] *Hewlett Packard 1997 Test and Measurement Catalog*, Santa Clara, CA, 1996, pp. 209-10.

[Hew97d] *HP 8360B Series Synthesized Swept Signal Generators - Technical Specifications*, via fax from Hewlett Packard Test and Measurement Call Center, Engelwood, CO, 1997.

[Hew97e] *Hewlett Packard 1997 Test and Measurement Catalog*, Santa Clara, CA, 1996, p. 303.

[Hew97f] *Microwave System Amplifiers - HP 83050A 2 to 50 GHz - Product Overview*, Hewlett Packard Company, Engelwood, CO, 1997.

[Hew97g] *RF & Microwave Test Accessories Catalog 1997/98*, Hewlett Packard Company, Santa Clara, CA, 1997, pp. 119-20.

[Huy90] C. Huygens, *Traité de la lumiere*, Leyden, 1690.

[Kel62] J.B. Keller, "Geometrical Theory of Diffraction," *J. Opt. Soc. of America*, vol. 52, no. 2, pp. 116-130, Feb. 1962.

[Kir82] Kirchhoff, "Zur Theorie der Lichsstrahlen," *Sitzangsberichte*, Academie Berlin, 1882.

[Kou74] R.G Kouyoumjian, and P.H. Pathak, "A Uniform Geometrical Theory of Diffraction for an Edge in a Perfectly Conducting Surface," *Proc. IEEE*, vol. 62, no. 11, pp. 1448-1461, Nov. 1974.

[Lue84] R.J. Luebbers, "Finite Conductivity Uniform GTD Versus Knife Edge Diffraction in Prediction of Propagation Path Loss," *IEEE Trans. Ant. and Propagat.*, vol. Ap-32, no. 1, pp. 70-76, Jan. 1984.

[Mag88] G.A. Maggi, "Sulla Propagazione libra e perturbata delle onde luminose in un mezzo isotropo," *Annali di Matematica*, vol. 16, pp. 21-48, 1888.

[Mic] *Microwave Development Company Catalog*, MDC, North Andover, MA, data sheet no. 8305008.

[Miy62a] K. Miyamoto and E. Wolf, "Generalization of the Maggi-Rubinowicz Theory of Boundary Diffraction Wave, Part I," *J. Optical Soc. of America*, vol. 52, no. 6, pp. 615-625, 1962.

[Miy62b] K. Miyamoto and E. Wolf, "Generalization of the Maggi-Rubinowicz Theory of Boundary Diffraction Wave, Part II," *J. Optical Soc. of America*, vol. 52, no. 6, pp. 626-637, 1962.

[Mum68] W.W. Mumford and E.H. Scheibe, *Noise Performance Factors in Communications Systems*, Horizon House - Microwave, Inc., Dedham, Mass., 1968.

[Neu58] H.E.J. Neugebauer and M.P. Bachynski, "Diffraction by Smooth Cylindrical Mountains," *Proc. IRE*, vol. 46, pp. 1619-1627, Sep. 1958.

[New04] I. Newton, *Optiks*, London, 1704.

[Rap96] T.S. Rappaport, *Wireless Communications*, Upper Saddle River, NJ: Prentice-Hall, 1996.

[Rub17] A. Rubinowicz, "Die Beugungswelle in der Kirchhoffschen Theorie der Beugungserscheinungen," *Annalen der Physik*, vol. 53, no. 4, pp. 257-278, 1917.

[Rub24] A. Rubinowicz, "Zur Kirchhoffschen Beugungstheorie," *Annalen der Physik*, vol. 73, no. 4, pp. 339-364, 1924.

[Rus92] T.A. Russell, "*Predicting Microwave Diffraction in the Shadows of Buildings*, master's thesis, Virginia Polytechnic Institute and State University, Blacksburg, VA, 1992.

[Sch33] J.C. Schelleng, C.R. Burrows, and E.B. Ferrell, "Ultra-short wave propagation," *Bell Syst. Tech. J.*, pp. 125-161, Apr. 1933.

[Sei95] S.Y. Seidel and H.W. Arnold, "Propagation measurements at 28 GHz to investigate the performance of local multipoint distribution service (LMDS)", IEEE Globecom Conference, 1995, pp. 754-757

[Som96] A. Sommerfeld, "Mathematische Theorie der Diffraction," *Mathematische Annalen*, vol. 47, S319, pp. 317-374, 1896.

[Sto49] G. Stokes, "Dynamical theory of diffraction," *Trans. Of the Cambridge Philosophical Society*, vol. 9, 1849

[Tho87] W. Thomson (Lord Kelvin), "On the Wave Roduced by a Ingle Impulse in Water of any Depth, or in a Dispersive Medium," *Philosophical Magazine*, vol. 23, no. 142, pp. 252-255, 1887.

[Uti97] *Utiflex ® Flexible Microwave Cable Assemblies Catalog*, UTI Corporation, Collegeville, PA, 1997, pp. 4,6,9.

[Vio88] E. Violette, R. Espeland, K. Allen, *Millimeter-Wave Propagation Characteristics and Channel Performance for Urban-Suburban Environments*, NTIA Report 88-239, Dec. 1988.

[Vir97] *Course Notes for EE 5655 Communication System Design*, Virginia Polytechnic Institute and State University, Blacksburg, VA, 1997

[You01] T. Young, "On the Theory of Light and Coulors," *Philosophical Transactions of the Royal Society*, vol. 92, pp. 12-49, 1801.

7. Vita

Peter A. Tenerelli was born in Plainfield, NJ, on June 25, 1967. He received his Bachelor of Science degree in Electrical Engineering from Virginia Polytechnic Institute and State University in 1990. Since 1990, Mr. Tenerelli has been employed by LCC International, Inc. of McLean, Virginia where is Project Manager of New Technologies. His experience includes the design, deployment and optimization of mobile radio networks, including the first digital cellular system in Germany. Most recently, he has been involved in developing engineering solutions for point to multipoint radio systems such as LMDS.

Mr. Tenerelli is a member of the IEEE.